THE JOURNAL OF COMPARATIVE NEUROLOGY 452:324–333 (2002)

Granule Neurons Generated During Development Extend Divergent Axon Collaterals to Hippocampal Area CA3

NICHOLAS B. HASTINGS,* MALIKA I. SETH, PATIMA TANAPAT, TRACY A. RYDEL, AND ELIZABETH GOULD
Department of Psychology, Princeton University, Princeton, New Jersey 08544

ABSTRACT

Most excitatory intrahippocampal pathways are characterized by significant, highly ordered projections into the long, or septotemporal, hippocampal axis. However, the mossy fiber system, the excitatory projection by which the dentate gyrus projects to hippocampal area CA3, is considered an exception, being organized to innervate exclusively transversely oriented cortical layers of the hippocampus. In the present study, the anatomy of the rat mossy fiber system was investigated using axonal tracing techniques, with an emphasis on determining its projection pattern into the long hippocampal axis. To this end, we used dual ipsilateral retrograde tracer injections to determine whether individual granule cells extend divergent axon collaterals to septotemporally distinct levels of hippocampal area CA3. We combined this technique with the fluorescent immunohistochemical detection of 5-bromo-2′-deoxyuridine (BrdU), a marker of granule cell precursors and their progeny, to address whether the divergence of mossy fiber collaterals within area CA3 might by related to ontogenic gradients in granule cell genesis. We observed single granule neurons that had retrogradely transported both tracers, indicating that they had axon collaterals passing through or terminating within the distinct levels of area CA3 into which tracer had been injected. By using BrdU labeling, we identified divergent granule neurons that were produced during embryonic and postnatal development. We observed no adult-generated granule neurons with significantly diverging mossy fiber collaterals. However, many fewer cells were labeled with BrdU in adult-exposed animals. Because of this smaller sample, we cannot rule out the possibility that small numbers of divergent adult-generated granule cells exist. We conclude that a proportion of the hippocampal mossy fiber projection extends septotemporally divergent axon collaterals to hippocampal area CA3. J. Comp. Neurol. 452:324–333, 2002.

Indexing terms: mossy fiber; retrograde tracing; granule cell; dentate gyrus

Modern neuroanatomical studies have consistently demonstrated that significant, highly organized septotemporal projections are characteristic of excitatory intrahippocampal pathways (Lorente de No, 1934; Hjorth-Simonsen, 1973; Swanson et al., 1978; Witter et al., 1989; Ishizuka et al., 1990; for review see Amaral and Witter, 1989, 1995). As a result, traditional models of hippocampal function stressing the functional independence of adjacent hippocampal "lamellae" (Andersen et al., 1971) have been supplanted by contemporary perspectives that emphasize the divergent neural connectivity and integrative information processing of the hippocampus (for review see Amaral and Witter, 1989; Amaral, 1993). In this light, it is surprising that studies of the hippocampal mossy fiber projection system, the excitatory pathway by which the dentate gyrus innervates hippocampal area CA3, have yielded little evidence of an extralamellar or even overtly topographic organization (Claiborne et al., 1986).

The hippocampal mossy fiber system comprises the dentate gyrus granule neurons, their axons (the mossy fibers

*Correspondence to: Nicholas B. Hastings, Department of Psychology, Green Hall, Washington Road, Princeton, NJ 08544.
E-mail: hastings@princeton.edu

Received 31 August 2001; Revised 23 April 2002; Accepted 27 June 2002.
DOI 10.1002/cne.10386
Published online the week of September 16, 2002 in Wiley InterScience (www.interscience.wiley.com).

proper), and various target cell populations (Gaarskjaer, 1986). The mossy fibers descend from the granule cell layer (gcl) to enter the hilus, wherein they ramify extensively to form a dense plexus of axon collaterals (Golgi, 1886; for review see Gaarskjaer, 1986; Claiborne et al., 1986). The hilar mossy fiber plexus contacts mossy cells (Ribak et al., 1985), inhibitory basket cells (Ribak and Seress, 1983), and probably a number of unidentified cell types (Claiborne et al., 1986; Amaral and Witter, 1995). The principal axons continue into Ammon's horn, coursing throughout much of the radial extent of proximal area CA3 as transversely oriented and largely unramifying fiber bundles (Blackstad et al., 1970; Gaarskjaer, 1978a; but see Claiborne et al., 1986). These bundles then collect to form the prominent stratum lucidum, within which the mossy fibers pass through and innervate the remaining distal portion of CA3.

Although early studies emphasized the predominantly transverse orientation of the hippocampal mossy fiber system (Ramon y Cajal, 1893; Lorente de No, 1934; Blackstad et al., 1970), both the classical and the contemporary literature include descriptions of the mossy fibers assuming a more oblique course within distal area CA3, by which they project along the septotemporal hippocampal axis (Ramon y Cajal, 1893; Lorente de No, 1934; McLardy, 1960; Blackstad et al., 1970; Swanson et al., 1978; Gaarskjaer, 1978a, 1981). In the rat, the oblique orientation of the mossy fiber system is difficult to observe using traditional histological techniques. Thus, the course and innervation pattern of the mossy fibers within CA3 of this species have been determined inferentially by studying the terminal points of the projection system (Blackstad, 1963; Blackstad et al., 1970; Swanson et al., 1978; Gaarskjaer, 1978a, 1981). In this regard, axonal tracing studies have proved useful not only in demonstrating the existence of septotemporally directed mossy fibers in the rat but also in investigating their topographic organization. The distribution of labeled granule neurons following the injection of retrograde axonal tracers into CA3 reveals that the total population of mossy fibers originating from a given level of the gcl forms a fanning pattern of innervation; mossy fibers are distributed to septal and, more prominently, to temporal portions of CA3. These studies also suggest that the extent to which individual mossy fibers extend, or "diverge," into the longitudinal axis may be related to the postmigrational position of their originating granule neurons (Gaarskjaer, 1978b, 1981). The septotemporal spread of mossy fibers appears to be greater when the axons originate from earlier-formed, laterosuperior regions of the gcl compared with more medioinferior regions.

Collectively, the results of previous studies suggest that the hippocampal mossy fiber system of the rat comprises both transversely and longitudinally directed components, the latter of which may contribute a topographically organized innervation of septotemporally oriented segments of area CA3. At the same time, these studies raise an issue of fundamental importance concerning the anatomic underpinnings of hippocampal mossy fiber divergence. Do the axons of a local ensemble of granule cells each project to different portions of CA3, or do individual granule neurons elaborate axons collaterals that are then distributed to distinct levels of the septotemporal axis (cf. Amaral and Witter, 1989; Fig. 1)?

In the present work, we have investigated this issue by using dual ipsilateral retrograde tracer injections. Furthermore, to determine whether axonal divergence might be related to the developmental age of granule neurons, we have combined retrograde tracing with the immunohistochemical detection of 5-bromo-2′-deoxyuridine (BrdU), a marker of proliferating cells and their progeny (Cameron and McKay, 2001).

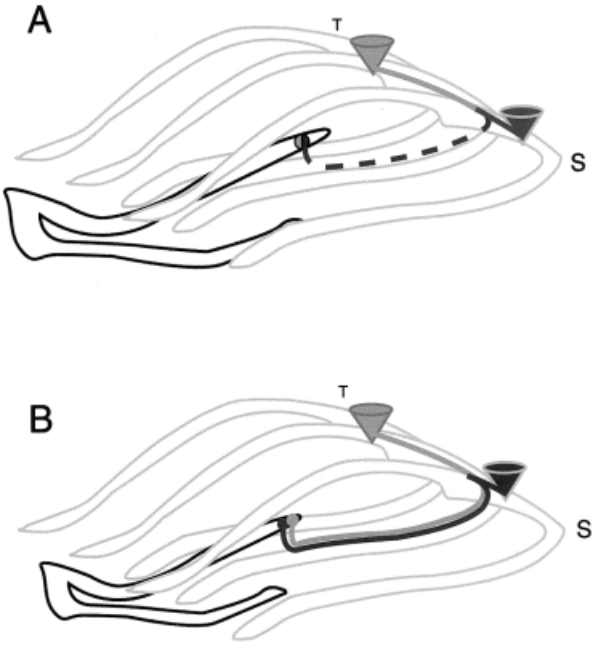

Fig. 1. Two, not necessarily mutually exclusive, models of mossy fiber divergence. **A:** The axon (dashed line) of a single granule neuron extends collaterals into the longitudinal hippocampal axis that terminate within distinct septotemporal levels of hippocampal area CA3. **B:** Two juxtaposed granule neurons each send a single unramified axon into the longitudinal hippocampal axis. Each axon terminates within a different septotemporal level of CA3. The cones depicted in area CA3 of each diagram represent ipsilateral retrograde tracer injection sites, the temporal (T) and septal (S) injections being of a light gray and dark gray tracer respectively. Retrograde dye transport results in the coincident labeling of a single granule neuron in A, and the single labeling of two granule neurons in B.

MATERIALS AND METHODS

Animal care and treatments

Male Sprague Dawley rats were exposed to BrdU during development either in utero, by injecting timed-pregnant dams (200 mg/kg BW in vehicle; saline with 0.007 N NaOH; i.p.) on embryonic day 17 (E17; n = 4) or by direct intraperitoneal injection (200 mg/kg BW in vehicle) on postnatal day 5 (P5; n = 4). Additional male rats were multiply injected with BrdU as adults (200 mg/kg BW, i.p./2 hours, total of six injections per animal) on postnatal day 60 (P60; n = 12). Multiple injections were carried out to increase the labeling of granule neuron precursors and the resulting sample size of adult-generated cells.

E17 and P5 animals were injected with the axonal retrograde tracers fast blue (FB) and dextran-conjugated tetramethylrhodamine (fluororuby; FR) upon reaching P60 (59 and 55 days after BrdU injection, respectively). Rats injected with BrdU on P60 were subsequently injected

with retrograde tracers 7 days (P60-7d; n = 6), 21 days (P60-21d; n = 3), or 55 days (P60-55d; n = 3) later.[1] An additional three rats were exposed to BrdU and injected with tracers at an interinjection distance (ID) great enough to prevent coincident retrograde transport. These animals were used to probe the maximal divergence of mossy fiber collaterals.

All subjects were derived from animals originally obtained from Taconic Farms (Germantown, NY). Animals were housed and handled in accordance with Institutional Animal Care and Use Committee guidelines, with specifications outlined in the National Institutes of Health *Guide for the Care and Use of Laboratory Animals*. Tap water and food (Purina Rat Chow) were freely available, and animals were maintained on a 12:12 hour light:dark cycle at 72°F, with 50% humidity.

Retrograde tracer injections

Animals were injected with atropine sulfate (40 μg/kg BW, s.c.) and then anesthetized with sodium pentobarbital (Nembutal; 65 mg/kg BW, i.p.). Incision sites were treated pre- and postoperatively with topical xylocaine (4.0%). All drugs were obtained from Henry Schein, Inc. (Melville, NY).

Anesthetized animals were placed in a small animal stereotaxic frame (model 900, David Kopf Instruments, Tujunga, CA) in the flat skull position. FB (2.0% in sterile isotonic saline; Sigma, St. Louis, MO) and FR (10.0% in sterile isotonic saline; Molecular Probes Inc., Eugene, OR) were pressure-injected through small, stereotaxically placed craniotomies. Both tracers were aimed at the distalmost portion of dorsal hippocampal area CA3, slightly lateral to the pyramidal cell field, to minimize damage to transversely oriented intrahippocampal fibers of passage.

Bilateral FB injections (50 nl) were placed at the following coordinates (in mm): AP –3.30, LM ±3.60, DV –3.10, with the syringes angled 0.50° laterally. Bilateral FR injections (80 nl) were placed at one of three different septotemporal levels to provide varied IDs (in mm): 1) AP −4.00, LM ±4.70, DV ±4.00; 2) AP −4.40, LM ±4.80, DV −4.00; and 3) AP −4.80, LM ±4.80, DV −4.50 (Fig. 2). Injections were placed with 1 μl Hamilton syringes held in dual model 960 Kopf electrode manipulators. Because mossy fiber projections are ipsilateral (Blackstad et al., 1970; Swanson et al., 1978), each unilateral pair of injection sites and the associated gcl labeling were examined as a separate case. In only one instance (a P60-7d subject) were two cases derived from a single animal.

Histological procedures

Perfusion and sectioning. Previous studies have determined that a 3 day survival time is sufficient for the complete retrograde transport of FB and FR from distal area CA3 to the dentate gyrus (Stanfield and Trice, 1988; Hastings and Gould, 1999). Animals were therefore deeply anesthetized with Nembutal (100 mg/kg BW, i.p.) 3 days after stereotaxic surgery and transcardially perfused with 4.0% paraformaldehyde in phosphate buffer, pH 7.4, at 4°C. The brains were then removed from the cranium, postfixed for 3 days in fresh perfusate at 4°C, and then sectioned on an oscillating tissue slicer. Transverse sections orthogonal to the anteroposterior axis (coronal sections) were taken through the entire hippocampus at 40 μm thickness, and the tissue sections were collected into a bath of 0.1 M Tris-buffered saline (TBS), pH 7.6, containing 0.2 mmol sodium azide.

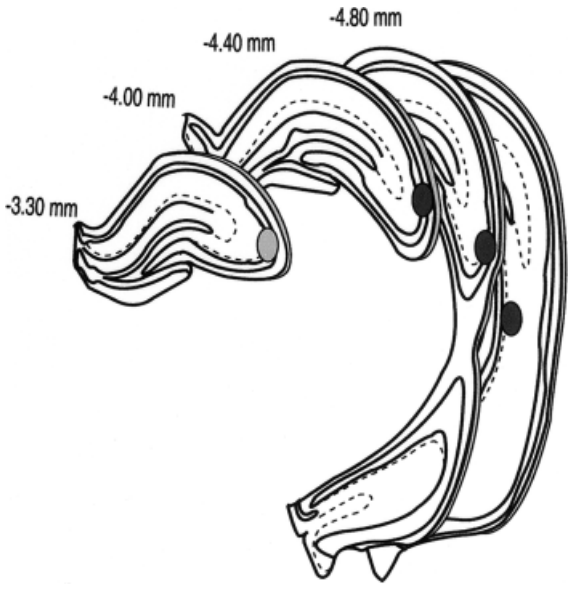

Fig. 2. Schematic drawings of transverse sections orthogonal to the anteroposterior axis of the hippocampal formation. The approximate anteroposterior position relative to bregma is indicated. The location and the relative scale of the tracer injection sites are represented by shaded ellipses, light gray for fast blue and dark gray for fluororuby. Labeling of important anatomic features is provided on a representative coronal section (Fig. 3B).

Alternate sections were mounted onto Superfrost Plus slides (Fisher Scientific, Pittsburgh, PA), dried, and examined for appropriate injection placement and retrograde transport of tracer into the ipsilateral gcl. The results of the current study are derived from a total of 20 brains (see above), each having retrograde tracer injections of comparable size, in which each injection was nonoverlapping and was confined to distal area CA3 and in which the ID was sufficient to result in some sections containing coincident retrograde transport of both tracers to the gcl.

BrdU and GFAP immunohistochemistry. For BrdU fluorescence immunolabeling, mounted sections were air dried, digested in trypsin (0.01% in Tris buffer containing 0.1% $CaCl_2$) for 20 minutes, denatured in 2 N HCl for 30 minutes, rinsed in TBS, and incubated overnight at room temperature in rat monoclonal antibody raised against BrdU (1:100 + 0.5% Tween-20; Accurate, Westbury, NY). The sections were then rinsed, incubated in secondary rat antisera conjugated to the fluorochrome Alexa-488 (1:500; Molecular Probes) for 30 minutes, and then coverslipped under 25.0% glycerol in TBS.

[1]By 7 days after BrdU injection, the number of BrdU-labeled cells in the dentate gyrus of rats is maximal (Gould et al., 1999), and many of the new neurons are expected to have extended axons to distal area CA3 (Hastings and Gould, 1999). Twenty-one days after BrdU injection, adult-generated granule neurons exhibit various morphological and biochemical characteristics of mature granule cells (Cameron et al., 1993; Gould and Tanapat 1997; Gould et al., 1999). Finally, because the E17 and P5 groups experienced an extensive period of time between BrdU and tracer injections, we also tracer injected a group of animals 55 days after BrdU exposure.

As in previous studies (Gould and Tanapat, 1997; Gould et al., 1999; Tanapat et al., 1999), we used BrdU peroxidase immunolabeling to determine stereological estimates of the total numbers of BrdU-labeled cells in the dentate gyrus. The peroxidase method was also used to map the location of BrdU-labeled cells within the gcl. A one-in-twelve coronal series of sections taken from three representative brains per experimental group was mounted and air dried, incubated in 0.1 M citric acid for 5 minutes at 90°C, digested in trypsin (0.05% in Tris buffer containing 0.1% $CaCl_2$) for 10 minutes, denatured in 2 N HCl for 30 minutes, rinsed in 0.1 M phosphate-buffered saline (PBS; pH 7.4), and incubated overnight at 4°C in mouse monoclonal antibody raised against BrdU (1:200 + 0.5% Tween-20; Novocastra, Newcastle Upon Tyne, United Kingdom). The sections were then rinsed in PBS, incubated in biotinylated secondary mouse antisera (1:200; Vector, Burlingame, CA) for 60 minutes, rinsed in PBS, incubated in avidin-biotin-horseradish peroxidase (AB; 1:100; Vector) for 60 minutes, rinsed in PBS, and reacted for 10 minutes in 0.01% diaminobenzidine (DAB) with 0.003% H_2O_2. The sections were then counterstained with cresyl violet, dehydrated, and coverslipped under Permount. As in previous work, the total number of immunolabeled cells was determined using a modified version of the optical fractionator method (West et al., 1991; Gould et al., 1999; Tanapat et al., 1999). Briefly, all BrdU-labeled cells in the gcl were counted on every twelfth section throughout the dentate gyrus at 400×, omitting cells located in the outermost plane of focus. For cell mapping, the position of all BrdU-labeled cells located within the gcl of the dorsal dentate gyrus [anteroposterior coordinates approximately –2.00 to –4.50 mm (Paxinos and Watson, 1986)] was recorded.[2]

In some cases, alternate sections were processed for GFAP immunofluorescence, providing a reliable means of determining regions in which tracer was passively incorporated. For glial fibrillary acidic protein (GFAP) immunolabeling, mounted sections were incubated in goat anti-GFAP (1:3,000; Santa Cruz Biotechnologies, Santa Cruz, CA) for 2 days at 4°C, rinsed in TBS, and then incubated in secondary goat antisera conjugated to Alexa-488 (1:500; Molecular Probes) for 30 minutes. The sections were rinsed in TBS and coverslipped under 25.0% glycerol in TBS.

Data acquisition and analysis

Data were collected using an Olympus BX60F reflected/transmitted light microscope (NY/NJ Scientific, Inc., Middlebush, NJ). The microscope was equipped with an LEP biopoint automated stage controller and a Heidenhain transducer (Ludl Electronic Products Ltd., Hawthorne, NY). Image capture was performed using an Optronics (Optronics Inc., Goleta, GA) DEI-750D CE digital camera and output box set and an Integral Flashpoint AGP video capture card. Data were collected and analyzed on a PC using the Neurolucida and Stereoinvestigator (v. 2000) data acquisition software modules from Microbrightfield Inc. (Colchester, VT). In some cases, images were captured using a Zeiss LSM-510 confocal microscope (Thornwood, NY).

Serial reconstruction

By using fluorescence microscopy (400×), we observed and recorded the three-dimensional position of two classes of granule cells, those incorporating both FB and FR retrograde tracers (FB^+/FR^+) and those that had incorporated both tracers and were additionally immunopositive for BrdU. Injection sites were recorded by contouring the maximal radial extent of the tracer diffusion zone, using GFAP immunofluorescence and the incidence of $GFAP^+/FB^+$ or $GFAP^+/FR^+$ cells as a guide for determining where the passive diffusion of tracer into cells was evident.

Wire-frame models of each subject brain were constructed using computer-assisted contouring of appropriate anatomic features, after which the contours were registered using the traced anatomic landmarks. The completed wire-frame models could be freely rotated through all three axes, allowing the distance of each mapped granule cell from the tracer injection sites to be determined relative to the true septotemporal axis of the hippocampus.

Statistical methods

We performed statistical analysis of the distribution of FB^+/FR^+ granule cells on brains that had relatively large IDs. With the selection of large IDs, analysis could be restricted to double-labeled granule cells with cell bodies located between the injection sites, while including cells with a wide distribution of axonal divergences. The distance along the hippocampal septotemporal axis of every FB^+/FR^+ granule cell located between the tracer injection sites was determined relative to the septalmost border of the caudal (FR) tracer injection. The distribution of double-labeled cell bodies was tested using the Kolmogorov-Smirnov single classification test for fitting continuous sample distributions. The d_{max} statistic for this test is reported using 5% critical values of g_δ with $\delta = 0.5$. Post hoc analysis of these results included computation of distribution skew and determination of whether the skew deviated significantly from zero (a symmetric distribution). This statistic and the (two-tailed) t value are reported.

Analysis of the cell maps was performed as follows. The gcl of each coronal section examined was partitioned into 20 bins of equal area, 10 in the transverse dimension, with each then subdivided into superficial and deep halves. The position of each BrdU-labeled cell was recorded, and, using the log-likelihood ratio test, we tested whether the observed BrdU-labeled cells were distributed with equal probability among the bins. The G-test statistic is reported with its associated degrees of freedom and was compared with critical values of χ^2 with $\alpha = 0.05$. Partitioned G-values for main and interaction effects were examined and are presented where appropriate.

RESULTS

Retrograde tracer injection sites and appearance of tracer diffusion zones

FB and FR injection sites consisted of two concentric zones of fluorescence. Immediately below the termination

[2]Because of the position of tracer injections and the resulting pattern of overlapping retrograde tracer transport, this region of the dentate gyrus gcl approximates the relevant sample space for the study (see also Fig. 3A).

of the needle track, a relatively small, bright zone of fluorescence typically surrounded a region of obvious tissue damage. A larger, more diffuse zone of fluorescence extended radially from the smaller zone but was not associated with evidence of tissue damage (Fig. 3B; see also Gaarskjaer, 1981; Hastings and Gould, 1999). Within both zones of fluorescence, cells exhibiting gross morphologic characteristics of neurons and glia appeared to incorporate retrograde tracer. Cells labeled by both GFAP immunohistochemistry and retrograde tracer were confined to these zones, suggesting that the passive uptake of tracer was restricted to the radial extent of the diffusion zone.

Patterns of retrograde transport resulting from the injection of tracers into distal area CA3

Injections placed in distal area CA3 resulted in labeling of the entire transverse extent of CA3, most likely via the associational fibers of this region, but did not label area CA1. There was no evidence for transsynaptic anterograde or retrograde transport. Within the dentate gyrus, discrete labeling of granule neurons was evident. Both cytoplasmic incorporation and nuclear incorporation of FB were observed (Fig. 3D–F), with labeling often evident in the proximal portions of dendrites. Incorporation of FR was restricted to the cytoplasm, including the proximal segments of dendrites and axons. FR incorporation was distinctly punctate, resulting in a mottled or speckled appearance of labeled neurons (Fig. 3C,E,F). Tracer diffusion from labeled neurons either into extracellular spaces or into adjacent, unlabeled neurons or glia was not observed with the postinjection survival times used.

Successful injection into distal area CA3 resulted in a distinctive pattern of retrograde transport to the gcl of the ipsilateral dentate gyrus that was similar for both tracers (Fig. 3A). In the rostralmost labeled sections, granule cells that had incorporated tracer were observed in the dorsal tip of the suprapyramidal blade of the gcl well septal to the injection level. Superficial portions of the infrapyramidal blade and more medial and ventral aspects of the suprapyramidal blade exhibited tracer incorporation in more caudal tissue sections. The greatest extent of tracer incorporation was observed slightly rostral to or coincident with the level of the injection site, often including the entire transverse extent of the gcl. Caudal to the level of injection, tracer labeling was typically restricted to middle portions of both blades of the dentate gyrus and often included the crest of the gcl, although scattered cells in the superior aspect of the suprapyramidal blade were often observed well posterior to the injection site. As a result of these patterns, granule cells exhibiting incorporation of both retrograde tracers could be present throughout the gcl but were most likely to be found in the laterosuperior aspect of the gcl (Fig. 3A).

Experimental manipulation of the FR injection site (Fig. 2) resulted in a varied degree of retrograde tracer overlap in the gcl. The area of the gcl in which overlapping tracer incorporation was evident was inversely correlated with ID, being more extensive in brains where the FB and FR injections were placed relatively close together. In three brains, the ID was great enough to prevent the coincident retrograde transport of tracer to the gcl. Among these brains, the smallest ID was approximately 1,700 μm.

Identification and distribution of double retrograde tracer-labeled granule cells

Granule cells in which the incorporation of both FB and FR was colocalized (FB^+/FR^+) were observed in all experimental groups (Fig. 3E). However, although most (but not all) granule cells located in regions of tracer overlap exhibited retrograde transport of either FB or FR, few granule cells in these regions were observed to have incorporated both retrograde tracers (see Table 1). The density of FB^+/FR^+ cells appeared to vary inversely with ID, being on average higher for small IDs (ID $<$ 450 μm; five brains, mean density 6.1 $\pm$ 1.25 cells per section) than for medium-sized (450 $<$ ID $<$ 750 μm; seven brains, mean density 4.2 $\pm$ 0.75 cells per section) and large (ID $>$ 750 μm; eight brains, mean density 1.1 $\pm$ 0.21 cells per section) IDs. Additionally, the density of FB^+/FR^+ cells varied systematically within subject brains, being lowest at septotemporal positions near either injection site and tending to peak at septotemporal positions approximately midway between the radial extent of each injection site. Peak cell densities were highest for small (7.8 $\pm$ 1.24) and medium-sized (9.7 $\pm$ 2.12) IDs and lower for large (3.6 $\pm$ 0.80) IDs.

The distribution of FB^+/FR^+ cells within the gcl was related to tracer ID (Fig. 4A). For brains in which the ID was relatively large, FB^+/FR^+ granule cells were observed only in the laterosuperior aspect of the suprapyramidal blade of the gcl. For medium IDs, FB^+/FR^+ cells were again observed in the laterosuperior aspect of the suprapyramidal blade but were also observed in more medioinferior regions of the suprapyramidal blade and, occasionally, in the laterosuperior aspect of the infrapyramidal blade. FB^+/FR^+ granule cells were observed in all regions of the gcl, including medioinferior aspects of the infrapyramidal blade and the crest of the gcl in brains having relatively small IDs.

We observed that the total number of FB^+/FR^+ granule cells tended to decrease with increasing ID (Fig. 4B). Extrapolation of this relationship predicted a theoretical ID of 1,945 μm, at which point only a single cell would be likely to incorporate both retrograde tracers. This figure agrees reasonably well with our empirical observations; we failed to observe FB^+/FR^+ granule cells in brains with IDs greater than 1,700 μm.

In brains with large IDs, the distances of FB^+/FR^+ granule cells from the FR injection site were found to be approximately normally distributed (Kolmogorov-Smirnov $d_{max} = 0.04$, $P > 0.05$). The distribution was not significantly skewed [observed $g_1 = -0.25$ vs. expected $g_1 = 0.00$, $t_{s(\infty)} = -1.09$, $P > 0.05$].

BrdU-labeling experiments

The greatest number of labeled cells was observed in animals exposed to BrdU on E17 (Table 1). The most heavily labeled of these generally exhibited a speckled appearance and were localized predominantly to the superficial aspect of both blades. Lightly labeled cells, presumably the late-generated progeny of granule cell progenitors incorporating BrdU on E17, were observed throughout the radial extent of the gcl (see Fig. 3G).

Large numbers of labeled cells were also observed in animals injected with BrdU on P5. These cells were also lightly speckled in appearance, but, in comparison with the case in E17 animals, the heavily labeled cells tended to

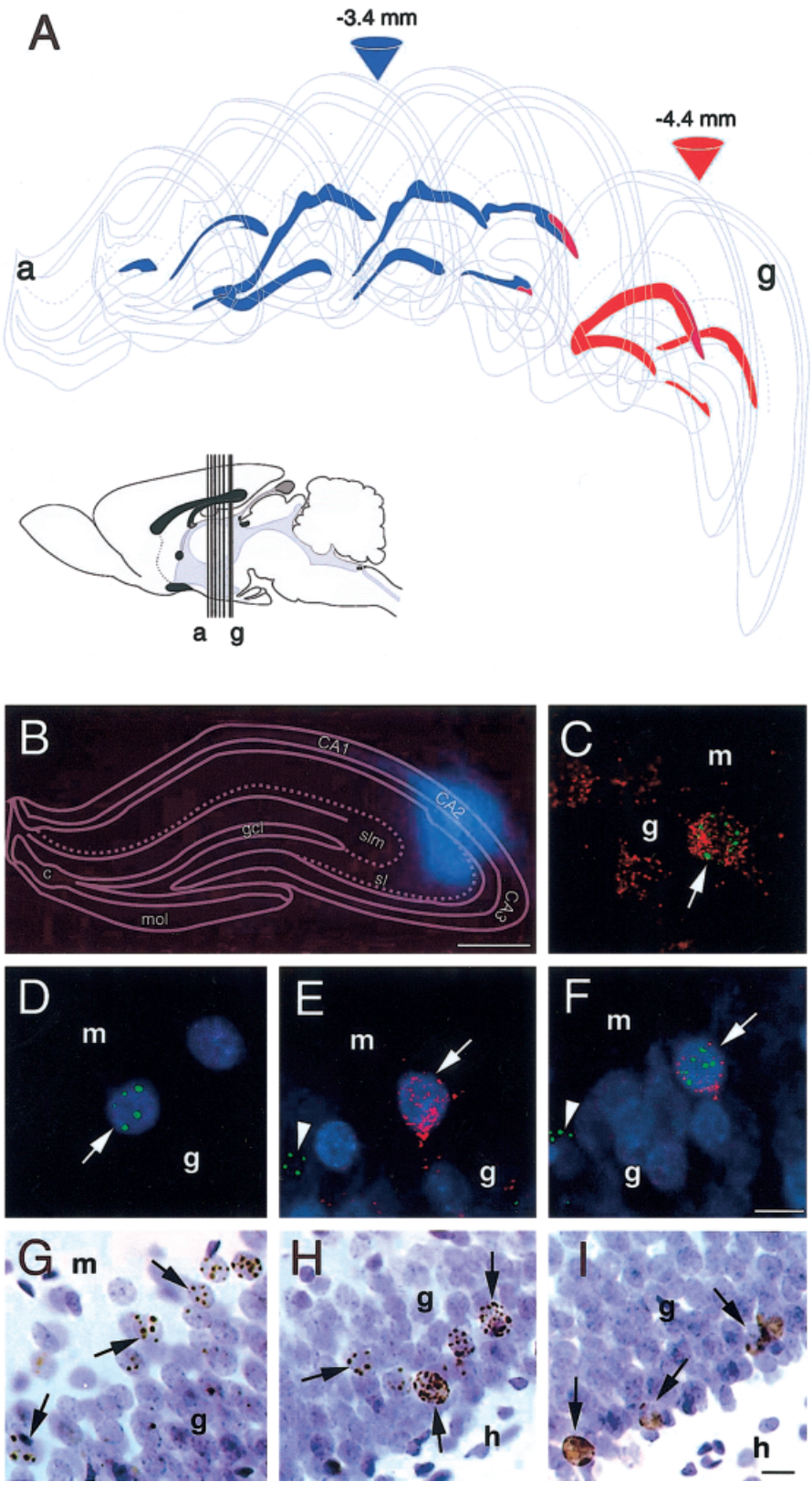
A
-3.4 mm
-4.4 mm
a
g
a g
B
CA1
CA2
CA3
gcl
slm
sl
c
mol
C
m
g
D
m
g
E
m
g
F
m
g
G m
g
H
g
h
I
g
h

Figure 3

TABLE 1. Mean Number of $BrdU^+$, FB^+/FR^+, and $BrdU^+/FB^+/FR^+$ Cells Observed for Each Experimental Group

	BrdU-labeled cells		Interinjection distance		FB^+/FR^+ granule cells[2]		$FB^+/FR^+/BrdU^+$ granule cells	
Group	Mean	SEM	Mean	SEM	Mean	SEM	Mean	SEM
E17	128,634	13,895.7	718.5	187.38	49.5	11.93	10.5	4.21
P5	63,010	7,145.5	585.8	21.42	64.8	21.42	5.5	2.23
P60-7d	6,512[1]	1,041.5[1]	834.2	144.58	18.2	3.44	0.0	—
P60-21d	5,000[1]	657.2[1]	707.0	296.42	29.7	12.67	0.0	—
P60-55d	4,163[1]	859.6[1]	1,059.0	204.69	14.7	5.04	0.0	—

[1]Data from multiple injections (see text).
[2]All animals received FB and FR injections as adults.

be more evenly distributed throughout both the transverse and the radial extents of the gcl (Fig. 3H).

Much smaller but still substantial numbers of BrdU-labeled cells were observed in all groups of experimental animals injected with BrdU as adults (P60). Cells were generally more heavily labeled in animals exposed to BrdU as adults than during development, with the reaction product typically filling the entire nucleus (Fig. 3I). This was true in P60-55d animals, suggesting that the observation is not attributable to a shorter survival time in the adult-injected groups. In P60-21d and P60-55d animals, the labeled cells tended to be relatively large and rounded. Labeled cells were more numerous, tended to be more heavily labeled, and were often irregularly shaped in P60-7d animals.

In P60-7d [G_{total} (19) = 489.30, $P < 0.05$], P60-21d [G_{total} (19) = 523.38, $P < 0.05$], and P60-55d [G_{total} (19) = 441.90, $P < 0.05$] experimental groups, quantitative analysis revealed that adult-generated cells were nonrandomly distributed. Partitioning of the total G value indicated significant clustering with respect to both the transverse [P60-7d, G(9) = 54.51; P60-21d, G(9) = 84.15; P60-55d, G(9) = 63.09; all $P < 0.05$] and radial [P60-7d, G(1) = 412.92; P60-21d, G(1) = 399.96; P60-55d, G(1) = 360.77; all $P < 0.05$] dimensions of the gcl. Collectively, adult-generated cells were preferentially located toward the middle portion of each blade of the gcl, rather than in the tips of the blades (particularly that of the suprapyramidal blade), and in the deep half of the gcl (Fig. 5).

$BrdU^+/FB^+/FR^+$ granule cells were observed in animals that had been exposed to BrdU on E17 (four brains, 42 $BrdU^+/FB^+/FR^+$ cells observed; see Fig. 3F) and P5 (four brains, 22 total cells). Although both $BrdU^+/FB^+$ and $BrdU^+/FR^+$ cells were observed in rats injected with BrdU as adults (P60), we did not observe any $BrdU^+/FB^+/FR^+$ granule cells in P60-7d, P60-21d, or P60-55d animals. However, it is important to note that much lower numbers of cells were BrdU-labeled in animals injected with the DNA synthesis marker as adults (e.g., P60-55d, 4,163 ± 859.6 cells) compared with animals that were injected on P5 (63,010 ± 7,145.5 cells) or exposed to BrdU in utero on E17 (128,634 ± 13,895.7 cells). Insofar as the smaller sample of $BrdU^+$ cells present in adult injected animals decreases the likelihood of observing triple-labeled neurons, it remains possible that divergent adult-generated granule neurons were not detected by our methods.

DISCUSSION

In this study, we examined the longitudinal projection topography of the hippocampal mossy fiber pathway by injecting the retrograde tracers FB and FR into distinct septotemporal levels of area CA3. The coincident incorporation of both tracers by many granule neurons and the

Fig. 3. (Overleaf.) **A:** Series of schematic transverse sections through the level of the hippocampus depicting representative patterns of retrograde dye transport resulting from the injection of fast blue (FB; blue) and fluororuby (FR; red) into area CA3. The diagram approximates the results for a medium interinjection interval. Regions of dye overlap resulting from the coincident retrograde transport of both tracers are shown in purple in A. The approximate locations of each tracer injection are at top. See B for identification of anatomic features in the sections. **Inset:** Sagittal view of the rat brain showing the approximate anteroposterior level of each of the transverse sections, a–g. **B:** Photomicrograph of a coronal section at the level of a representative FB injection site. The contours of additional features of the section have been traced for reference. c, Crest of the dentate gyrus; CA1–CA3, pyramidal cell fields of Ammon's horn; gcl, granule cell layer of the dentate gyrus; mol, molecular layer; sl, stratum lucidum; slm, stratum lacunosum moleculare. **C–F:** Confocal laser scanning microscope images (1,200×) of tracer-labeled and BrdU-labeled granule neurons in the dentate gyrus of an adult rat receiving BrdU on E17 and injected with the retrograde tracers FB and FR on P60. Animals were perfused 3 days after tracer injection. Retrograde transport of FR [red (appearing pink when colocalized with FB)] results in punctate labeling of the cytoplasm, often including proximal neurites, but does not generally label the nucleus. Incorporation of FB (blue), on the other hand, results in a more diffuse labeling that typically includes the nucleus. BrdU immunolabeling (green) has been visualized using the fluorochrome Alexa-488. **C:** Several granule neurons labeled with FR, one of which is also immunopositive for BrdU (arrow). **D:** Two granule neurons labeled with FB, one of which is also immunopositive for BrdU (arrow). **E:** FB-labeled granule neurons, including one that has also incorporated FR (arrow). Arrowhead indicates a single BrdU-labeled cell. **F:** A cell that has incorporated both FB and FR and is immunopositive for BrdU (arrow). Arrowhead indicates a single BrdU-labeled cell. **G–I:** Brightfield photomicrographs (400×) of BrdU-labeled cells in the suprapyramidal blade of the rat dentate gyrus. The cell layer has been counterstained with cresyl violet. **G:** BrdU-labeled cells in a rat that was injected on E17 and killed on P63. Numerous lightly labeled cells are located throughout the gcl, with the most heavily labeled cells (examples indicated with arrows) located in its superficial aspect. **H:** BrdU-labeled cells in a rat injected on P5 and killed on P63. Fewer labeled cells (examples indicated by arrows) are noted overall, and these tend to be located in the middle to deep aspects of the gcl. **I:** BrdU-labeled cells in a rat multiply injected with BrdU on P60 and killed 58 days later. BrdU-labeled cells (examples indicated by arrows) are darkly labeled and located in the deep aspect of the gcl. g, Granule cell layer; h, hilus; m, molecular layer of the dentate gyrus. Scale bar in B = 600 μm. Scale bar in F (for photomicrographs C–F) and I (for photomicrographs G–I) = 12.5 μm.

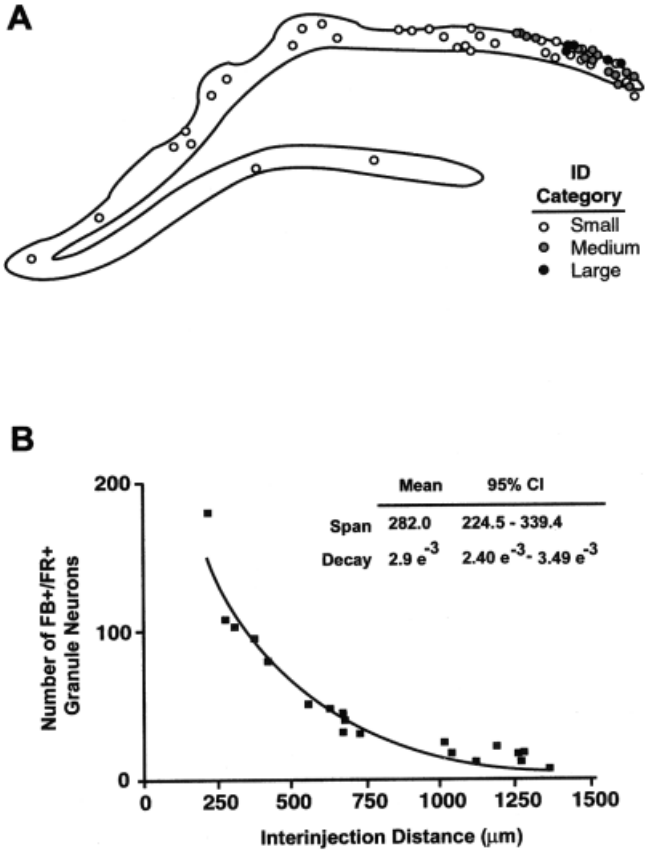

Fig 4. Distribution and numbers of fast blue- and fluororuby-positive granule cells. **A:** Representative outline of the dentate gyrus in a transverse section taken through the hippocampus approximately –3.80 mm from bregma. In each of the experimental brains, all double-labeled granule cell bodies were located between the tracer injection sites at this level. The locations of granule cells that have incorporated both fast blue and fluororuby are depicted and shaded to indicate whether the mapped position was observed in brains that have large, medium-sized, or small tracer IDs (ID Category). In brains having large IDs, the location of FB^+/FR^+ granule cells is restricted to the superior aspect of the tip of the suprapyramidal blade of the gcl. In brains having relatively small IDs, FB^+/FR^+ cells may be found throughout the gcl. **B:** Relationship between tracer ID and the numbers of granule cells incorporating both fast blue and fluororuby retrograde tracers. The data have been fit with an exponential decay model in which the number of FB^+/FR^+ cells is constrained to plateau at zero. Mean values and 95% confidence intervals for the fit parameters are provided. The regression predicts a maximal divergence of mossy fiber collaterals within area CA3 of approximately 1,900 μm. In the present study, we observed brains in which the ID was great enough that no granule cells were doubly labeled. Among these brains, the smallest ID was approximately 1,700 μm.

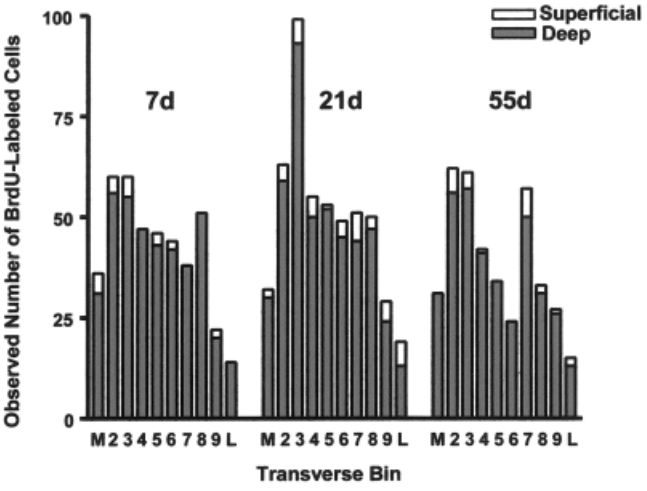

Fig 5. Distribution of adult-generated granule neurons within the gcl. Three representative brains from each of the P60-7d, P60-21d, and P60-55d experimental groups were analyzed. Bars represent the cumulative distribution of BrdU-labeled cells into each of 20 bins (see Materials and Methods). Regardless of the survival time after BrdU injection, the distribution of adult-generated cells was nonrandom. BrdU-labeled cells were clustered in the middle and deep portions of each blade, away from the latero- and mediosuperior aspects of the gcl.

septotemporal localization of double-labeled cell bodies between the injection sites indicated that a proportion of this cell population elaborates axon collateral branches that project along and diverge within the longitudinal hippocampal axis.

Previous work has suggested that mossy fiber divergence within CA3 might be related to ontogenic gradients in granule cell genesis, migration, and integration within the incipient gcl (Gaarskjaer, 1986). We explored this issue through systematic manipulation of septotemporal IDs within CA3. We observed that the distribution of FB and FR double-labeled granule cells varied in a predictable fashion as a function of tracer ID, the postmigrational position of highly divergent granule neurons being consistent with that of granule cells formed early in the ontogeny of the gcl. Studies combining axonal tracing with the immunohistochemical detection of BrdU, a marker of proliferating cells and their progeny (Cameron and McKay, 2001), further demonstrated that the granule neurons elaborating the most highly divergent mossy fiber axon collaterals were most likely to have been formed during embryonic or postnatal development.

A proportion of granule neurons in the dentate gyrus extends axon collaterals that project to different septotemporal levels of hippocampal area CA3

Anterograde terminal degeneration and retrograde tracing studies provided the first recent evidence that the hippocampal mossy fiber projection may in fact have a septotemporally divergent as well as a topographic component (Blackstad et al., 1970; Gaarskjaer, 1978a, 1981; for review see Gaarskjaer, 1986). To date, however, the anatomic substrate for mossy fiber "divergence" has remained obscure (Fig. 1).

In the present study, we observed granule neurons exhibiting the coincident incorporation of FB and FR. Serial reconstruction and three-dimensional mapping of the position of tracer-labeled granule neurons confirmed that many of the FB^+/FR^+ cell bodies were located within levels of the dentate gyrus that lay between the radial extent of the two tracer injection sites. A single, unbranching mossy fiber originating from this septotemporal level is unlikely to have taken up both tracers. We confirmed that the passive tracer uptake zones resulting from dye injection were restricted to the target region and did not

impinge directly on any portion of the dentate gyrus. Moreover, we observed, in the gcl, both tracer-labeled and nontracer-labeled granule cells adjacent to one another, suggesting that transported tracer was not likely to have diffused among neighboring granule cells. Our injection sites unavoidably involved fibers of passage within the alveus and the strata oriens and radiatum of Ammon's horn. However, these fiber tracts are not known to originate within the dentate gyrus, and we observed neither anterograde nor transynaptic retrograde transport of FB or FR, indicating that granule neurons were not likely to have been labeled indirectly. Because granule neurons extend a single primary axon, these results collectively indicate that the coincident retrograde transport of FB and FR occurred by way of axonal collateral branches projecting to, and likely terminating within, the septotemporally distinct CA3 injection sites.

The patterns of singly retrogradely labeled granule cells resulting from either FB or FR injection observed in the present study were similar to those described in previous reports using single retrograde tracer injections into CA3 (cf. Gaarskjaer, 1981). The level at which the entire transverse extent of the gcl incorporated tracer was typically found somewhat rostral to the level of the corresponding tracer injection. Additionally, tracer incorporation was observed to appear first in, and recede last from, the laterosuperior portions of the gcl. The mossy fiber pathway therefore appears to have a generally transverse and slightly temporal trajectory, with the bending of mossy fibers from this course being most pronounced when the axons originate from the laterosuperior aspect of the gcl.

Interestingly, we found that the distribution of granule cells extending divergent mossy fiber collaterals to CA3 was centered in gcl levels lying roughly midway between the FB and FR injection sites, implying that the length of septally and temporally directed mossy fiber axon collaterals is roughly equivalent. Thus, it would appear that, although the mossy fiber pathway generally exhibits an asymmetric temporal trajectory, a portion of the pathway, perhaps only that contributed by granule neurons extending axon collaterals to CA3, is more symmetrically divergent. The underlying mechanisms that specify symmetric divergence in a portion of the mossy fiber pathway are unknown.

Correlations between time of production, postmigrational position, and divergence of granule cells extending axon collaterals to area CA3

In rodents, distinct spatiotemporal patterns in granule cell neurogenesis and migration guide the formation of the gcl and the outgrowth of the hippocampal mossy fiber system during development (see Gaarskjaer, 1985, and references therein; Schlessinger et al., 1975; Bayer, 1980a, b). In general, the first granule neurons derived from the ventricular neuroepithelium form the most superficial and lateral aspects of the suprapyramidal blade. This laterosuperior aspect of the suprapyramidal blade appears relatively mature at birth and grows during the postnatal period by the addition of granule cells to more medial and successively deeper portions of the gcl (Gaarskjaer, 1985). During the postnatal development of the gcl, the addition of subsequent granule cells from a secondary hilar proliferative matrix (Bayer and Altman, 1974; Bayer, 1980b) occurs without a marked transverse gradient. The migration of postnatally formed granule neurons is, however, radially organized, such that more recently generated granule cells migrate to successively deeper portions of the cell layer (Bayer, 1980b). Granule neurons continue to be produced and integrated into the gcl throughout adulthood (Altman, 1962a, b; for a recent review see Tanapat et al., 2001). Adult-generated granule cells may be observed throughout the gcl (cf. Kuhn et al., 1996). However, detailed descriptions of their patterns of migration and final integration sites in the adult rat hippocampus have not been published.

Previous studies have suggested that the histogenetic gradients of gcl formation guide the longitudinal projection topography of hippocampal mossy fibers (Gaarskjaer, 1981; for review see Gaarskjaer, 1986). The present results also suggest that the divergence of mossy fiber collateral branches within area CA3 may also be related to the transverse and radial position, and hence the developmental age, of their originating granule neurons. We observed that the number and distribution of FB^+/FR^+ granule neurons changed as a function of the septotemporal distance between FB and FR tracer injections. In brains in which the ID was relatively small, more FB^+/FR^+ granule neurons were observed and were located throughout both blades and crest of the gcl. However, in brains in which the ID was relatively large, few FB^+/FR^+ granule cells were observed, and these were restricted to the laterosuperior tip of the suprapyramidal blade.

The results of combined axon-tracing and BrdU-labeling studies indicated that some granule neurons extending highly divergent mossy fiber axon collaterals were formed during embryonic or postnatal development, insofar as we found a number of $BrdU^+/FB^+/FR^+$ granule neurons in the gcl of rats exposed in utero or on P5. However, although adult-generated granule neurons are known to extend axons to area CA3 (Stanfield and Trice, 1988; Markakis and Gage, 1999; Hastings and Gould, 1999), we did not observe triple-labeled granule neurons in any animals exposed to BrdU as adults. It is critical to point out that the inability to find adult-generated cells with divergent mossy fibers may be a function of the markedly smaller BrdU-labeled sample in this group. In addition, however, we observed clustering in the distribution of adult-generated cells in the deep and medial aspects of both the supra- and the infrapyramidal blades of the gcl. These positional biases were maintained for up to 55 days following BrdU exposure (Fig. 5), well after adult-generated granule cells are known to exhibit a mature phenotype (Cameron et al., 1993; Gould and Tanapat, 1997; Kempermann et al., 1997) and, presumably, have ceased migration. Thus, the inability to observe triple-labeled cells in rats exposed to BrdU as adults may also be related to gradients in the migration and integration of adult-generated granule neurons.

Although our data cannot conclusively rule out the possibility that adult-generated granule neurons extend divergent axon collaterals to area CA3, it is possible that mossy fiber divergence exists solely as an attribute of granule neurons produced during perinatal development. If this is true, then mossy fiber divergence may be an inherent attribute of granule neurons formed during various periods in development. However, it would seem more likely that divergence occurs secondarily to the development of area CA3. In this way, for example, axon collat-

erals that initially terminate in spatial proximity could ultimately become divergent through the radial growth of the CA3 terminal field. Finally, it remains possible that septotemporally divergent mossy fiber collaterals are elaborated during both developmental and adult hippocampal neurogenesis but that adult-generated mossy fiber collaterals are more likely to be pruned. Developmental remodeling of axon collateral branches is common among many developing populations of cells, including those of the hippocampus (see Gomez-Di Cesare et al., 1997, and references therein) and could operate within the developing and adult hippocampus to determine septotemporal mossy fiber branching patterns. Given that the survival of adult-generated granule neurons is highly dependent on experiential factors (Gould et al., 1999; for review see Hastings et al., 2001), this proposal is particularly intriguing and raises the possibility that projection patterns of adult-generated granule neurons may be similarly influenced by the environment.

ACKNOWLEDGMENTS

This work was supported by NIH grants MH12362 (N.B.H.) and MH52423 (E.G.).

LITERATURE CITED

Altman J. 1962a. Are new neurons formed in the brains of adult mammals? Science 135:1127–1128.

Altman J. 1962b. Autoradiographic study of degenerative and regenerative proliferation of neuroglia cells with tritiated thymidine. Exp Neurol 8:302–318.

Amaral DG. 1993. Emerging principles of intrinsic hippocampal organization. Curr Opin Neurobiol 3:225–229.

Amaral DG, Witter MP. 1989. The three-dimensional organization of the hippocampal formation: a review of anatomical data. Neuroscience 31:571–591.

Amaral DG, Witter MP. 1995. Hippocampal Formation. In Paxinos G, editor. The rat nervous system. San Diego: Academic Press. p 443–493.

Andersen P, Bliss TV, Skrede KK. 1971. Lamellar organization of hippocampal pathways. Exp Brain Res 13:222–238.

Bayer SA. 1980a. Development of the hippocampal region in the rat. I. Neurogenesis examined with ^{3}H-thymidine autoradiography. J Comp Neurol 190:87–114.

Bayer SA. 1980b. Development of the hippocampal region in the rat. II. Morphogenesis during embryonic and early postnatal life. J Comp Neurol 190:115–134.

Bayer SA, Altman J. 1974. Hippocampal development in the rat: cytogenesis and morphogenesis examined with autoradiography and low-level X-irradiation. J Comp Neurol 158:55–79.

Blackstad TW. 1963. Ultrastructural studies on the hippocampal region. Progr Brain Res 3:122–148.

Blackstad TW, Brink K, Hem J, Jeune B. 1970. Distribution of hippocampal mossy fibers in the rat. An experimental study with silver impregnation methods. J Comp Neurol 138:433–450.

Cameron HA, McKay RD. 2001. Adult neurogenesis produces a large pool of new granule cells in the dentate gyrus. J Comp Neurol 435:406–417.

Cameron HA, Woolley CS, McEwen BS, Gould E. 1993. Differentiation of newly born neurons and glia in the dentate gyrus of the adult rat. Neuroscience 56:337–344.

Claiborne BJ, Amaral DG, Cowan WM. 1986. A light and electron microscopic analysis of the mossy fibers of the rat dentate gyrus. J Comp Neurol 246:435–458.

Gaarskjaer FB. 1978a. Organization of the mossy fiber system of the rat studied in extended hippocampi. I. Terminal area related to number of granule and pyramidal cells. J Comp Neurol 178:49–72.

Gaarskjaer FB. 1978b. Organization of the mossy fiber system of the rat studied in extended hippocampi. II. Experimental analysis of fiber distribution with silver impregnation methods. J Comp Neurol 178:73–88.

Gaarskjaer FB. 1981. The hippocampal mossy fiber system of the rat studied with retrograde tracing techniques. Correlation between topographic organization and neurogenetic gradients. J Comp Neurol 203:717–735.

Gaarskjaer FB. 1985. The development of the dentate area and the hippocampal mossy fiber projection of the rat. J Comp Neurol 241:154–170.

Gaarskjaer FB. 1986. The organization and development of the hippocampal mossy fiber system. Brain Res Brain Res Rev 11:335–357.

Golgi C. 1886. Sulla fina anatomia degli organi centrali del sistema nervoso. Milano: U. Hoepli.

Gomez-Di Cesare CM, Smith KL, Rice FL, Swann JW. 1997. Axonal remodeling during postnatal maturation of CA3 hippocampal pyramidal neurons. J Comp Neurol 384:165–180.

Gould E, Tanapat P. 1997. Lesion-induced proliferation of neuronal progenitors in the dentate gyrus of the adult rat. Neuroscience 80:427–436.

Gould E, Beylin A, Tanapat P, Reeves A, Shors TJ. 1999. Learning enhances adult neurogenesis in the hippocampal formation. Nat Neurosci 2:260–265.

Hastings NB, Gould E. 1999. Rapid extension of axons into the CA3 region by adult-generated granule cells. J Comp Neurol 413:146–154.

Hastings NB, Tanapat P, Gould E. 2001. Neurogenesis in the adult mammalian brain. Clin Neurosci Res 1:175–182.

Hjorth-Simonsen A. 1973. Some intrinsic connections of the hippocampus in the rat: an experimental analysis. J Comp Neurol 147:145–161.

Ishizuka N, Weber J, Amaral DG. 1990. Organization of intrahippocampal projections originating from CA3 pyramidal cells in the rat. J Comp Neurol 295:580–623.

Kempermann G, Kuhn HG, Gage FH. 1997. More hippocampal neurons in adult mice living in an enriched environment. Nature 386:493–495.

Kuhn GH, Dickinson-Anson H, Gage FH. 1996. Neurogenesis in the dentate gyrus of the adult rat: age-related decrease of neuronal progenitor proliferation. J Neurosci 16:2027–2033.

Lorente de No R. 1934. Studies on the structure of the cerebral cortex. II. Continuation of the study of the ammonic system. J Psychol Neurol 46:113–177.

Markakis EA, Gage FH. 1999. Adult-generated neurons in the dentate gyrus send axonal projections to field CA3 and are surrounded by synaptic vesicles. J Comp Neurol 406:449–460.

McLardy T. 1960. Neurosyncytial aspects of the hippocampal mossy fibre system. Confin Neurol 20:1–17.

Paxinos G, Watson C. 1986. The rat brain in stereotaxic coordinates. New York: Academic Press.

Ramon y Cajal S. 1893. Estructura del asta de Ammon. Ann Soc Esp Hist Nat 22:53–114.

Ribak CE, Seress L. 1983. Five types of basket cell in the hippocampal dentate gyrus: a combined Golgi and electron microscopic study. J Neurocytol 12:577–597.

Ribak CE, Seress L, Amaral DG. 1985. The development, ultrastructure and synaptic connections of the mossy cells of the dentate gyrus. J Neurocytol 14:835–857.

Schlessinger AR, Cowan WM, Gottlieb DI. 1975. An autoradiographic study of the time of origin and the pattern of granule cell migration in the dentate gyrus of the rat. J Comp Neurol 159:149–175.

Stanfield BB, Trice JE. 1988. Evidence that granule cells generated in the dentate gyrus of adult rats extend axonal projections. Exp Brain Res 72:399–406.

Swanson LW, Wyss JM, Cowan WM. 1978. An autoradiographic study of the organization of intrahippocampal association pathways in the rat. J Comp Neurol 181:681–715.

Tanapat P, Hastings NB, Reeves AJ, Gould E. 1999. Estrogen stimulates a transient increase in the number of new neurons in the dentate gyrus of the adult female rat. J Neurosci 19:5792–5801.

Tanapat P, Hastings N, Gould E. 2001. Adult neurogenesis in the hippocampal formation. In: Nelson CA, Luciana M, editors. Handbook of developmental cognitive neuroscience. Cambridge, MA: MIT Press. p 93–105.

West MJ, Slomianka L, Gundersen HJ. 1991. Unbiased stereological estimation of the total number of neurons in the subdivisions of the rat hippocampus using the optical fractionator. Anat Rec 231:482–497.

Witter MP, Van Hoesen GW, Amaral DG. 1989. Topographical organization of the entorhinal projection to the dentate gyrus of the monkey. J Neurosci 9:216–228.